ACS APPLIED NANO MATERIALS

www.acsanm.org Article

Self-Assembled Mesoporous Zeolitic Imidazolate Framework-8 (ZIF-8) Nanocrystals Bearing Thiol Groups for Separations Technologies

Gustavo M. Segovia, Jimena S. Tuninetti, Omar Azzaroni,* and Matías Rafti*

Cite This: https://dx.doi.org/10.1021/acsanm.0c02376 Read Online

ACCESS | Metrics & More | Article Recommendations | Supporting Information

ABSTRACT: Colloidal suspensions of Zn-based ZIF-8 metal−organic framework (MOF) particles were synthesized (both micrometer μ-ZIF-8- and nanometer n-ZIF-8-sized, respectively). Postsynthetic modification was carried using 2-amino-ethanethiol (cysteamine or Cys), a thiol-bearing monodentate ligand, and particles obtained were employed for the assembly of films on gold-coated electrode surfaces. The results obtained show that, aside from conferring chemical affinity toward Au, when suitable molar ratios are employed, cysteamine modification causes partial coordinative chemical etching of inherently microporous ZIF-8 units, thus giving rise to additional mesoporosity. Cysteamine concentration and exposure time were found to act as control parameters ultimately determining the transport properties of porous films obtained, which can then feature, *e.g.*, size-exclusion effects. The colloidal modification strategies like the one hereby described can be employed for the preparation of robust nano-organized MOF thin films with hierarchical porosity, which bear great potential for its application in separation technologies.

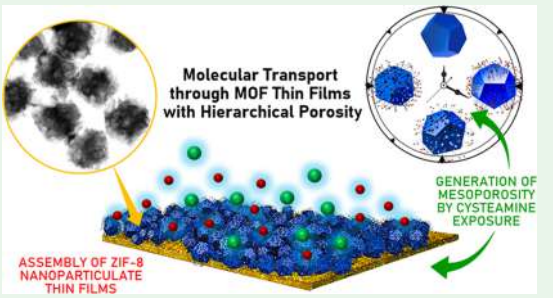

KEYWORDS: *MOFs, ZIF-8, cysteamine, microporosity, mesoporosity, colloidal synthesis, separations*

INTRODUCTION

Microporous coordination polymers or metal−organic frameworks (MOFs) can be best described as crystalline porous organic−inorganic solids built from the coordination of metal ions or metal-containing clusters with multidentate organic linkers.[1−6] This relatively novel family of materials feature high thermal and chemical stabilities, tailored porosity, and among the highest Brunauer−Emmett−Teller (BET) surface areas ever reported (7000 m^2/g).[7] Such interesting characteristics have rendered them promising candidates for use in diverse fields, *e.g.*, separations,[8,9] biomedicine,[10] hybrid materials,[11,12] catalysis,[13] sensing,[14,15] electrocatalysis,[16−18] energy conversion/storage,[19] and capture of greenhouse effect gases,[20,21] just to name a few. The quest for new MOFs suitable for emerging applications, and moreover, the research oriented to discover suitable synthetic paths and modification strategies allowing further control on key features such as size, chemical functionalization, and morphology, has gained increasing importance in the last few years.[22−24] For example, the widely used post- and presynthetic MOF modification strategies, oriented to the introduction of particular chemical moieties, have brought new perspectives for the creation of porous materials with tailored structure functionality.[12,25−28] Because of the above-described features, MOFs are appealing for their use in the fabrication of porous films, and are extensively employed for applications concerning energy storage and conversion or sensor-related technologies.[29,30] Many of the general strategies described in the abundantly available literature dealing with pore modification in bulk MOFs (although not extensively explored) are in principle valid for MOF films, *e.g.*, the creation of hierarchical porosity with template[31,32] and template-free synthesis methods,[33] postsynthesis chemical etching,[34−37] linker labilization,[13] use of mixed ligands,[38,39] and chemical modulators.[40−42] The application of such approaches renders films with tailored affinity, pore size, or stimuli responsivity, thus opening the path for the design of "smart" materials.[43,44]

Particularly interesting examples of the versatility of MOFs make use of ZIF-8, a prominent member of the zeolitic imidazolate frameworks (ZIFs) subclass. ZIF-8 can be straightforwardly synthesized, features relatively high thermal and chemical stabilities toward hydrolysis in aqueous environments, and received a great deal of attention in the last few years due to its exciting applications in diverse fields such as colloidal chemistry,[45] heterogeneous catalysis,[46] separation technologies,[47,48] sensors,[49] biomedicine,[50] and drug delivery.[51] The ZIF-8 structure can be described as an infinite ordered framework of tetrahedrally N-coordinated Zn^{2+} ions with 2-methylimidazolate, featuring intrinsic permanent micro-

Received: September 1, 2020
Accepted: October 9, 2020

porosity (11.6 Å diameter hydrophobic micropores).[52,53] It was recently shown that control on thickness, morphology, and chemical structure of films can be achieved using the liquid-phase epitaxy method and yields remarkable features like superprotonic conductivity.[54,55] An alternative approach for the construction of such porous films is by assembling predesigned MOF units,[56,57] which can be thus conveniently manipulated using colloidal chemistry toolbox (*e.g.*, for conferring tailored affinity for a given substrate surface or analyte).[58] Further characterization of interesting properties of such films (*e.g.*, transport properties) can be conveniently assessed with the cyclic voltammetry (CV) technique using suitable redox probes.[59,60]

In this work, we discuss the possibility of constructing nano-organized MOF thin films capable of tailoring and tuning the molecular transport across interfaces using predesigned, assemblable building blocks. Our nanoarchitectonic approach[61−63] takes advantage of the versatility of colloidal chemistry for surface functionalization of nano-objects, and exploits the effect of cysteamine postsynthetic modification of ZIF-8 units to create nanostructured, self-assembled films on gold substrates.[64−66] Aside from surface positioning of −SH moieties, as previously reported,[58] we observed that cysteamine molar ratios and exposure times used for ZIF-8 colloidal units modification can yield partial coordinative chemical etching, as evidenced by particle surface roughening. Moreover, such partial etching causes the appearance of additional (tunable) superimposed mesoporosity of ZIF-8 units, which can effectively modulate transport through the assembled porous media, a key feature for the design of novel materials for separation technologies.

EXPERIMENTAL SECTION

Reactants. Methanol (CH_3OH, Anedra, RA-ACS), zinc nitrate hexahydrate ($Zn(NO_3)_2{\cdot}6H_2O$, Sigma-Aldrich, 98%), 2-methylimidazole ($C_4H_6N_2$, Aldrich, 99%), cysteamine (C_2H_7NS, Acros Organics, 98%), 2-[4-(2-hydroxyethyl)piperazin-1-yl]ethanesulfonic acid (HEPES, $C_8H_{18}N_2O_4S$, Sigma, 99.5%), sodium formate (HCO_2Na, Sigma-Aldrich, >99%), potassium hexacyanoferrate(II) trihydrate ($K_4Fe(CN)_6{\cdot}3H_2O$, Biopack, 99.3%), potassium hexacyanoferrate-(III) ($K_3Fe(CN)_6{\cdot}3H_2O$, Anedra, 99.3%), and potassium chloride (KCl, Anedra, 99.8%) were used for the experiments hereby described.

Synthesis Methods. *Synthesis of Micrometer-Sized ZIF-8 (μ-ZIF-8).* ZIF-8 microcrystals (μ-ZIF-8) were synthesized via a solvothermal method by adding 750 mg of zinc nitrate (4 mmol), 648 mg of 2-methylimidazole (8 mmol), and 200 mg of sodium formate (3 mmol) in 60 mL of dry methanol, for final concentrations of 67, 133, and 50 mM, respectively (ZIF-8 stoichiometric (metal/linker) ratio, 1:2). The synthesis mixture was immersed for 1 min in an ultrasonic bath and then transferred to a stainless steel Teflon-lined autoclave for 24 h at 100 °C. The obtained product was separated from solution by repeated cycles of centrifugation (15 min and 6000 rpm) and redispersion in fresh solvent. After separation, the final powdered product was vacuum-dried.

Synthesis of Nanometer-Sized ZIF-8 (n-ZIF-8). ZIF-8 nanocrystals (n-ZIF-8) were obtained by mixing appropriate volumes of 50 mM zinc nitrate and 100 mM 2-methylimidazole methanolic stock solutions to yield 2-methylimidazole excess ((metal/linker) molar ratio, 1:5). The nanocrystals obtained after 1 h reaction period at room temperature were separated from the synthesis solution via centrifugation and redispersion in methanol. The gravimetric concentration of n-ZIF-8 in the final dispersion was approximately 1.5 mg/mL.

Postsynthetic Modification. Depending on whether cysteamine modification was carried out in micrometer-sized or nanometer-sized ZIF-8 colloidal suspensions, different conditions were applied. For μ-ZIF-8 suspensions, (linker/modulator) (Hmim/Cys) ratios of (1500:1), (150:1), (15:1), and (5:1) were used with a constant agitation exposure time of 7 days at room temperature. For n-ZIF-8, the suspensions obtained were exposed to a fixed (Hmim/Cys) molar ratio of 150:1, corresponding to the highest Cys content that still yields stable colloidal n-ZIF-8 suspensions. Exposure periods explored were 6, 9, 48, and 168 h, and the modification process was stopped in all cases by separation using centrifugation and redispersion with fresh solvent cycles.

n-ZIF-8 + Cys Film Assembly of Nanometer-Sized Units on Gold-Coated Conductive Substrates. The modified n-ZIF-8 + Cys nanocrystals colloidal suspension (1.5 mg/mL) was employed for film assembly via simple room-temperature dip-coating over clean Au conductive substrates. After a 5 h contact time, the substrates were repeatedly washed by immersion in fresh methanol to remove excess MOF nanocrystals noncovalently attached via thiol moieties exposed.

RESULTS AND DISCUSSION

Both nano- and micrometer-sized ZIF-8 units were post-synthetically modified using different (Hmim/Cys) molar ratios and contact times. Micrometer-sized ZIF-8 units featuring low area/volume ratios were employed to explore the effect of high cysteamine molar ratios on cysteamine modification (*i.e.*, to overcome the already discussed limitation imposed by the stability range of nanometer-sized ZIF-8 units).[58] Micrometer-sized ZIF-8 units were modified with increasingly higher cysteamine molar proportions using a fixed 7-day contact time. The microcrystals obtained following such a procedure will be hereafter referred to as μ-ZIF-8 + Cys-*r*, where *r* stands for Hmim in the (Hmim/Cys) molar ratio of 1.

The insight gained from a thorough analysis of the effect of cysteamine modification on ZIF-8 micrometer-sized units was then used for understanding the materials obtained when applying such a modification procedure on nanometer-sized MOF units (n-ZIF-8) for a fixed (Hmim/Cys) molar ratio of 150:1 and incremental exposure times (hereafter referred to as n-ZIF-8 + Cys-*t*, with *t* representing the exposure time in hours). Modified n-ZIF-8 + Cys-*t* units were then used for the assembly of films over gold conductive substrates (Scheme 1), and the effect of cysteamine modification on film porosity was gauged in terms of film transport properties (via CV experiments with suitable redox probes) and N_2 adsorption experiments.

Wide-Angle X-ray Scattering (WAXS) and Transmission Electron Microscopy (TEM) Experiments. The

Scheme 1. Schematic Illustration of the Sequential Steps Leading to the Formation of ZIF-8 MOF Thin Films with Hierarchical Porosity

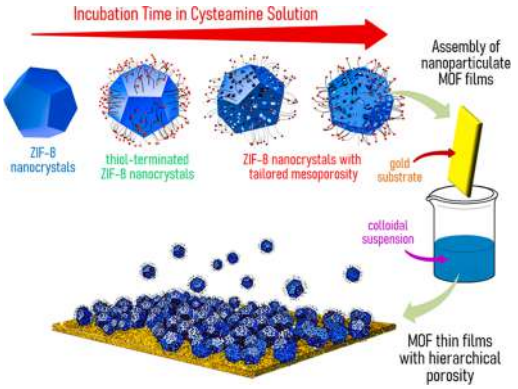

https://dx.doi.org/10.1021/acsanm.0c02376
ACS Appl. Nano Mater. XXXX, XXX, XXX−XXX

crystalline structure of materials obtained (both before and after exposure to different cysteamine molar ratios) was determined using powder wide-angle X-ray scattering (WAXS). The results obtained are presented in Figure 1,

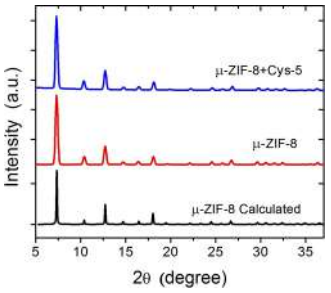

Figure 1. WAXS experimental results obtained for μ-ZIF-8 compared to the calculated diffractogram (black). μ-ZIF-8 (as-prepared material, red), and μ-ZIF-8 + Cys-5 (blue, obtained after modification with the highest Hmim/Cys molar ratio used, 5:1).

together with the expected diffractogram for ZIF-8 reported crystal structure. The evident agreement allows us to ensure the presence of the ZIF-8 phase both in the as-prepared sample and after modification using the highest cysteamine molar ratio explored, that is, μ-ZIF-8 + Cys-5 (with a Hmim/Cys ratio of 5:1). It should be expected then that such a molar proportion would yield a material with the nominal ZIF-8 microporosity (see N_2 adsorption experiments below). Additional WAXS experiments for the remaining synthesized materials can be found in the Supporting Information, together with TEM and Raman vibrational spectroscopy experiments, which provide further evidence on the conservation of MOF crystalline structure after cysteamine modification (see Figures S1−S3 in the Supporting Information).

Nitrogen Adsorption Isotherms. The surface area and porosity of the obtained materials were assessed with N_2 adsorption experiments performed before and after cysteamine modification. Figure 2 shows the isotherms corresponding to

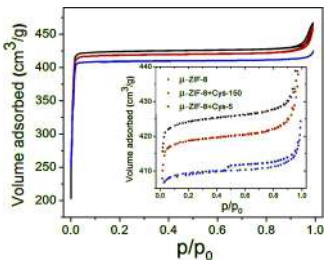

Figure 2. Nitrogen adsorption isotherms of μ-ZIF-8 (black line), μ-ZIF-8 + Cys-150 (red line), and μ-ZIF-8 + Cys-5 (blue line).

nonmodified μ-ZIF-8, μ-ZIF-8 + Cys-150, and μ-ZIF-8 + Cys-5. Aside from the typical shape of Type I isotherms corresponding to a microporous material such as ZIF-8 MOF, a subtle hysteresis loop ascribable to the presence of mesopores appears only for the highest cysteamine molar ratio used (*i.e.*, μ-ZIF-8 + Cys-5). The existence of such added porosity can cause dramatic changes in transport properties (see below), but it does not significantly affect the BET surface areas obtained, which depend mostly on the preserved intrinsic microporosity (in line with the WAXS experiments presented above, which suggest the preservation of ZIF-8 crystalline structure); see Table 1.

Table 1. Calculated BET Surface Areas from the Nitrogen Adsorption Isotherms Presented in Figure 2 for the As-Prepared Micrometer-Sized ZIF-8 Units, and after Modification with 150:1 and 5:1 Molar Ratios of Hmim/Cys

	μ-ZIF-8	μ-ZIF-8+Cys-150	μ-ZIF-8+Cys-5
BET area (m^2/g)	1210	1181	1158

Figure S4a shows the calculations of Barrett−Joyner−Halenda (BJH)[67] pore volume distributions (V_p), which are also in line with the suggested additional porosity appearing after modification for μ-ZIF-8+Cys-5. Calculations using the Dubinin−Radushkevich model for micropore capacities are presented in Figure S4b, with no significant differences with the above BET surface area calculations.

Nanometer-Sized ZIF-8 Units. Given that nanometer-sized objects are to be used as building units for film assembly, the effect of different exposure times for fixed (150:1) molar ratios (upper stability limit) on n-ZIF-8 units was explored. The BET surface area derived from N_2 isotherms for n-ZIF-8 + Cys-168 (maximum cysteamine exposure time explored, 168 h) is comparable to the corresponding value for cysteamine-modified micrometer-sized ZIF-8 units (1211 m^2/g), although the calculated pore size distribution shows some subtle differences (see Figure S5 in the Supporting Information). Additional evidence of the proposed cysteamine etching as responsible for the appearance of mesopores can be observed in the surface roughening of the otherwise smooth n-ZIF-8 units shown in TEM (Figure 3). From infrared spectra of modified particles,[58] the absence of stretching modes arising from free amine groups of cysteamine upon combination with ZIF-8 units suggests the occurrence of coordination with Zn^{2+} moieties as responsible for the mentioned etching.

Characterization of Films and Evaluation of Transport Properties. *Chemical and Morphological Characterization of Films Assembled via Thiolate−Gold Interactions.* Having established the effect of cysteamine modification on the porosity and structure of n-ZIF-8 units, films were assembled using such building units over conductive gold surfaces taking advantage of the proverbial thiol-Au affinity. CV experiments to characterize the role played by such interaction were carried out for different Au surfaces acting as working electrodes, namely: (i) covered by a chemisorbed cysteamine self-assembled monolayer (SAM), (ii) covered by a physisorbed bare n-ZIF-8 monolayer, and (iii) covered by a thiol-directed n-ZIF-8 + Cys-168 monolayer (*i.e.*, molar ratio, 150:1; contact time, 168 h) (see Supporting Information, Figure S6). CV peaks ascribable to thiol-reductive electrodesorption, positioned ≈ −900 mV *vs* Ag/AgCl reference potential electrode, are present only when thiolate (−SH) moieties mediate adsorption. This fact strongly suggests chemisorption of cysteamine-modified nanocrystals over Au surfaces. Such a hypothesis was further confirmed by AFM experiments carried out on films assembled with cysteamine-modified nanocrystals (see Figure 4, films corresponding to n-ZIF-8 + Cys-168). It can be clearly observed that the presence of n-ZIF-8 bundles completely covers the substrate surface, in line with observations made via CV experiments (see below). The film thickness can be estimated to be approximately 80

https://dx.doi.org/10.1021/acsanm.0c02376
ACS Appl. Nano Mater. XXXX, XXX, XXX−XXX

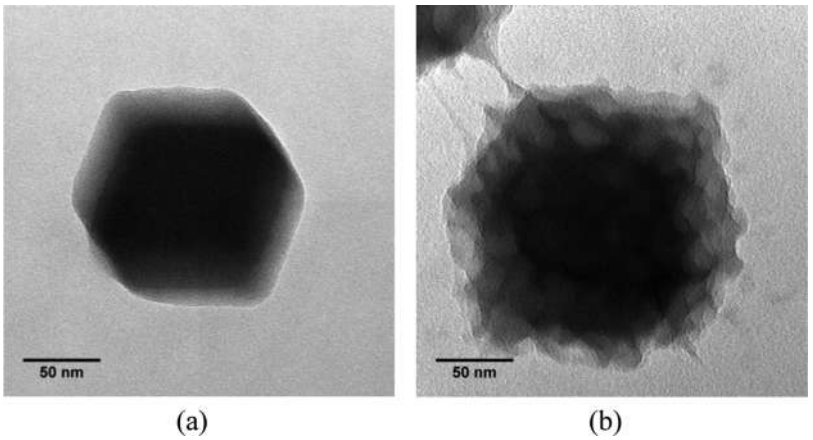

Figure 3. TEM images evidencing surface roughening caused by exposure of n-ZIF-8 to (150:1) cysteamine molar ratios for 168 h (n-ZIF-8 + Cys-168): (a) n-ZIF-8 and (b) n-ZIF-8 + Cys-168.

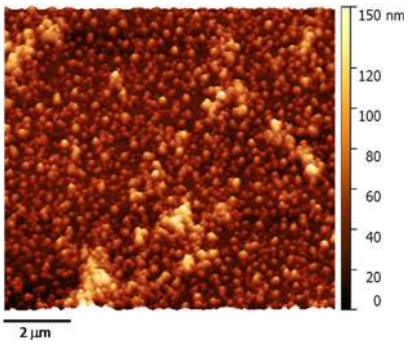

Figure 4. AFM micrograph ($10 \times 10\ \mu m^2$) of n-ZIF-8 + Cys-168 film assembled on gold-coated substrate.

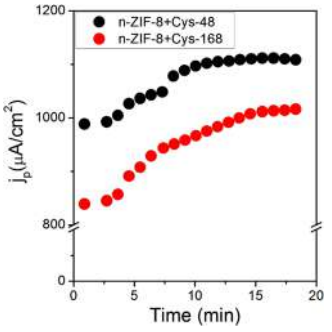

Figure 5. Temporal evolution of the anodic peak current density from CV experiments using n-ZIF-8 + Cys-48 (black) and n-ZIF-8 + Cys-168 (red) films assembled over gold substrates.

nm, based on the AFM height profile (see Figure S7 in the Supporting Information), which correlates nicely with what could be expected for a monolayer built from such thiolate-anchored MOF units, and dynamic light scattering (DLS) experiments (see Figure S8 in the Supporting Information). Additionally, both surface modification and concentration dependence of −SH moieties on cysteamine exposure time were demonstrated by following S and Zn signals in X-ray photoelectron spectroscopy, where an increase in the S/Zn signal ratio for 168 *vs* 48 h is observed (see XPS in Figures S9, S10, and Table S1).

Transport Properties of Films. Having established the effect of cysteamine modification regarding both decoration with −SH moieties enabling chemically directed film assembly and generation of additional mesoporosity, experiments oriented to determine the influence of such modifications on the transport properties of films were carried. A straightforward way for the evaluation of transport properties in films is by measuring the variation of apparent diffusion coefficients of suitable redox probes in CV experiments, *e.g.*, $Fe(CN)_6^{3-/4-}$.

Figure 5 shows the temporal evolution of the anodic peak current registered for films assembled using n-ZIF-8 + Cys-48 and n-ZIF-8 + Cys-168 units. The observed behavior can be understood considering that the diffusion path for redox probes through the film becomes increasingly intricate, as the exposure time to cysteamine (and thus chemical etching) of the units employed for the assembly increases from 48 to 168 h. This result is in line with the above-discussed experiments regarding both preservation of ZIF-8 crystal structure and the appearance of additional porosity caused by cysteamine (see the additional N_2 adsorption experiments presented in Figure S5 corresponding to n-ZIF-8 + Cys-168, as well as WAXS patterns in Figure S11 of the Supporting Information). It is important to note that ZIF-8 microporosity is not accessible to $Fe(CN)_6^{3-/4-}$ due to its molecular dimensions ($6 \times 6 \times 6$ Å^3 *vs* ZIF-8 nominal pore window size 3.4 Å).[68] Peak current plots allow us to clearly distinguish two stages in time evolution. An initial stage is characterized by a local minimum peak current ($t \approx 10$ min), in which probe diffusion is restricted due to hindered solvent permeation through the mesoscopic channels constituted by interparticle space shaped by cysteamine etched nanocrystals. Summarizing, cysteamine exposure can be used to modulate chemical etching of film building units, and thus ultimately providing an increasingly tortuous diffusion path.

The second stage of the observed time evolution starts once the solvent has already wetted the mesoporous space available, and thus redox probe diffusion becomes less restricted, reaching a maximum asymptotic current density limit value ($t \approx 15$−20 min). In this regard, such a complex interaction between (intrinsically hydrophobic) ZIF-8 porous environments and aqueous media and the possibility of modulation via postsynthesis modification were recently demonstrated by means of nuclear magnetic resonance experiments.[69]

Apparent diffusion coefficients of $Fe(CN)_6^{3-/4-}$ on the assembled films can be obtained applying the Randles−Sevcik analysis to the anodic peak current densities determined. Figure 6a shows the results obtained for the n-ZIF-8 + Cys-*t* films as cysteamine contact time *t* for nanoparticle

https://dx.doi.org/10.1021/acsanm.0c02376
ACS Appl. Nano Mater. XXXX, XXX, XXX−XXX

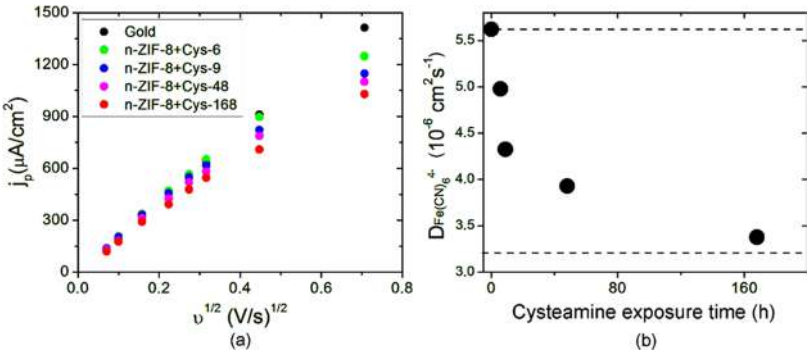

Figure 6. (a) Current density plots obtained from CV experiments performed using different n-ZIF-8 + Cys films prepared with building units exposed to cysteamine with increasing contact time. (b) Apparent diffusion coefficients calculated using the Randles−Sevcik equation and data from (a), where the dotted lines correspond to limit-case scenarios (see text).

modification *prior* to film assembly increases. The following expression was used

$$j_p = 0.4463nFC(nF/RT)^{1/2}\nu^{1/2}D^{1/2} \quad (1)$$

where n is the number of electrons transferred in the considered electrochemical process, F is the Faraday constant, C is the bulk concentration of redox probe, R is the ideal gas molar constant, and T is the absolute temperature. Apparent diffusion coefficients (D) can be derived from linear fits, as presented in Figure 6b, and the values obtained follow a pseudoexponential decay as modification exposure time increases. Again, such a decrease can be understood in terms of the effect of chemical etching, as discussed above (see the XPS experiments presented in Figures S9, S10, and Table S1 in the Supporting Information). The numerical values of apparent diffusion coefficients are also presented in Table S2 (see the Supporting Information).

The upper dotted line in Figure 6b corresponds to the diffusion coefficient value of the probe when using bare gold substrate (5.9×10^{-6} cm^2/s) that agrees well with the values reported in previous related studies.[70] The lowest apparent diffusion coefficient value obtained is compatible with the values reported for the experiments using the same redox probe in heterogeneously nucleated continuous ZIF-8 films grown over modified ITO conductive substrates (lower dotted line in Figure 6b).[60] The above-discussed similarities with limit-case scenarios suggest that the observed behavior for cysteamine-modified ZIF-8 building blocks (*i.e.*, a pseudoexponentially decaying apparent diffusion coefficient) is compatible with an increasingly higher tortuous path for the diffusing redox probe through the film, highly dependent in turn on the chemical etching caused by cysteamine exposure of preformed nano-ZIF-8 film units.

CONCLUSIONS

The above-described experiments demonstrate that, exposure of both micrometer-sized and nanometer-sized colloidal suspensions of metal−organic framework ZIF-8 units to monodentate linker cysteamine is a valid strategy for introducing additional controlled mesoporosity on an eminently microporous material such as ZIF-8 MOF, as further confirmed through CV and N_2 adsorption experiments. Direct evidence of the presence of surface-positioned thiol moieties on nanosized n-ZIF-8 + Cys units and the dependence of surface concentration on exposure time was obtained by XPS measurements.

Apparent diffusion coefficients of redox probes through the films were calculated using Randles−Sevcik equation. Results obtained can be rationalized having in mind the effects of cysteamine modification, *i.e.*, to add a superimposed mesoporosity via coordinative etching and to modulate the hydrophobic character of ZIF-8 porous matrix due to surface decoration. The observed control on apparent diffusion in the synthesized films resembles the principle behind size-exclusion chromatography extensively used in polymer science, with the interesting added feature of possible further chemical tuning of selectivity via surface chemistry. The hereby described strategy for controlling porosity (and thus tortuosity) of synthesized films bears great interest for diverse applications related to separation technologies, and with minor modifications can be adapted for different MOFs, thus allowing great control over porosity and chemistry of the pore walls.

ASSOCIATED CONTENT

Supporting Information

The Supporting Information is available free of charge at https://pubs.acs.org/doi/10.1021/acsanm.0c02376.

Characterization techniques and figures covering results of characterization techniques for μ-ZIF-8 + Cys and n-ZIF-8 + Cys films (PDF)

AUTHOR INFORMATION

Corresponding Authors

Omar Azzaroni − *Instituto de Investigaciones Fisicoquímicas Teóricas y Aplicadas (INIFTA), Fac. de Cs. Exactas, Universidad Nacional de La Plata - CONICET, 1900 La Plata, Argentina;* orcid.org/0000-0002-5098-0612; Email: azzaroni@inifta.unlp.edu.ar; http://softmatter.quimica.unlp.edu.ar

Matías Rafti − *Instituto de Investigaciones Fisicoquímicas Teóricas y Aplicadas (INIFTA), Fac. de Cs. Exactas, Universidad Nacional de La Plata - CONICET, 1900 La Plata, Argentina;* orcid.org/0000-0003-3393-358X; Email: mrafti@quimica.unlp.edu.ar

Authors

Gustavo M. Segovia − *Instituto de Investigaciones Fisicoquímicas Teóricas y Aplicadas (INIFTA), Fac. de Cs. Exactas, Universidad Nacional de La Plata - CONICET, 1900 La Plata, Argentina; Universidad Nacional de San Martín, B1650, Argentina*

https://dx.doi.org/10.1021/acsanm.0c02376
ACS Appl. Nano Mater. XXXX, XXX, XXX−XXX

Jimena S. Tuninetti − *Instituto de Investigaciones Fisicoquímicas Teóricas y Aplicadas (INIFTA), Fac. de Cs. Exactas, Universidad Nacional de La Plata - CONICET, 1900 La Plata, Argentina;* orcid.org/0000-0002-9813-1265

Complete contact information is available at: https://pubs.acs.org/10.1021/acsanm.0c02376

Notes

The authors declare no competing financial interest.

■ ACKNOWLEDGMENTS

M.R., J.S.T., and O.A. are CONICET staff members. G.M.S. acknowledges Jorge L. Llanos, Edgardo A. Fertitta, and Ethel S. Flores for the help and discussion regarding N_2 uptake experiments, and CONICET for a doctoral scholarship. Financial support from ANPCyT (PICT-2015-0239, PICT-2016-1680) and Universidad Nacional de La Plata (PPID-X016) is greatly acknowledged. The SAXS/WAXS system used (INIFTA) was obtained via "Nanopymes"-EuropeAid/132184 D/SUP/AR (Contract 331-896) project.

■ REFERENCES

(1) Hoskins, B.; Robson, R. Infinite Polymeric Frameworks Consisting of Three Dimensionally Linked Rod-like Segments. *J. Am. Chem. Soc.* **1989**, *111*, 5962−5964.
(2) Yaghi, O. M.; Li, H.; Davis, C.; Richardson, D.; Groy, T. L. Synthetic Strategies, Structure Patterns, and Emerging Properties in the Chemistry of Modular Porous Solids Decorated Diamond Nets: Porous Metal. *Acc. Chem. Res.* **1998**, *31*, 474−484.
(3) Li, H.; Yagui, O. M.; O'Keeffe, M.; Eddaoudi, M. Design and Synthesis of an Exceptionally Stable and Highly. *Nature* **1999**, *402*, 276−279.
(4) Rowsell, J. L. C.; Yaghi, O. M. Metal−Organic Frameworks: A New Class of Porous Materials. *Microporous Mesoporous Mater.* **2004**, *73*, 3−14.
(5) Férey, G. Hybrid Porous Solids: Past, Present, Future. *Chem. Soc. Rev.* **2008**, *37*, 191−214.
(6) Long, J. R.; Yaghi, O. M. The Pervasive Chemistry of Metal−Organic Frameworks. *Chem. Soc. Rev.* **2009**, *38*, 1213.
(7) Farha, O. K.; Eryazici, I.; Jeong, N. C.; Hauser, B. G.; Wilmer, C. E.; Sarjeant, A. A.; Snurr, R. Q.; Nguyen, S. T.; Yazaydin, A. Ö.; Hupp, J. T. Metal-Organic Framework Materials with Ultrahigh Surface Areas: Is the Sky the Limit? *J. Am. Chem. Soc.* **2012**, *134*, 15016−15021.
(8) Li, J. R.; Sculley, J.; Zhou, H. C. Metal-Organic Frameworks for Separations. *Chem. Rev.* **2012**, *112*, 869−932.
(9) Zhang, X.; Liu, Y.; Li, S.; Kong, L.; Liu, H.; Li, Y.; Han, W.; Yeung, K. L.; Zhu, W.; Yang, W.; Qiu, J. New Membrane Architecture with High Performance: ZIF-8 Membrane Supported on Vertically Aligned ZnO Nanorods for Gas Permeation and Separation. *Chem. Mater.* **2014**, *26*, 1975−1981.
(10) McKinlay, A. C.; Morris, R. E.; Horcajada, P.; Férey, G.; Gref, R.; Couvreur, P.; Serre, C. BioMOFs: Metal-Organic Frameworks for Biological and Medical Applications. *Angew. Chem., Int. Ed.* **2010**, *49*, 6260−6266.
(11) Giménez, R. E.; Piccinini, E.; Azzaroni, O.; Rafti, M. Lectin-Recognizable MOF Glyconanoparticles: Supramolecular Glycosylation of ZIF-8 Nanocrystals by Sugar-Based Surfactants. *ACS Omega* **2019**, *4*, 842−848.
(12) Allegretto, J. A.; Giussi, J. M.; Moya, S. E.; Azzaroni, O.; Rafti, M. Synthesis and Characterization of Thermoresponsive ZIF-8@PNIPAm-: Co-MAA Microgel Composites with Enhanced Performance as an Adsorption/Release Platform. *RSC Adv.* **2020**, *10*, 2453−2461.
(13) Yuan, S.; Zou, L.; Qin, J. S.; Li, J.; Huang, L.; Feng, L.; Wang, X.; Bosch, M.; Alsalme, A.; Cagin, T.; Zhou, H. Construction of Hierarchically Porous Metal-Organic Frameworks through Linker Labilization. *Nat. Commun.* **2017**, *8*, No. 15356.
(14) Stassen, I.; Burtch, N.; Talin, A.; Falcaro, P.; Allendorf, M.; Ameloot, R. An Updated Roadmap for the Integration of Metal-Organic Frameworks with Electronic Devices and Chemical Sensors. *Chem. Soc. Rev.* **2017**, *46*, 3185−3241.
(15) Sappia, L. D.; Tuninetti, J. S.; Ceolín, M.; Knoll, W.; Rafti, M.; Azzaroni, O. MOF@PEDOT Composite Films for Impedimetric Pesticide Sensors. *Glob. Challenges* **2020**, *4*, No. 1900076.
(16) Rafti, M.; Marmisollé, W. A.; Azzaroni, O. Metal-Organic Frameworks Help Conducting Polymers Optimize the Efficiency of the Oxygen Reduction Reaction in Neutral Solutions. *Adv. Mater. Interfaces* **2016**, *3*, 1−5.
(17) Mártire, A. P.; Segovia, G. M.; Azzaroni, O.; Rafti, M.; Marmisollé, W. Layer-by-Layer Integration of Conducting Polymers and Metal Organic Frameworks onto Electrode Surfaces: Enhancement of the Oxygen Reduction Reaction through Electrocatalytic Nanoarchitectonics. *Mol. Syst. Des. Eng.* **2019**, *4*, 893−900.
(18) Fenoy, G. E.; Scotto, J.; Azcárate, J.; Rafti, M.; Marmisollé, W. A.; Azzaroni, O. Powering Up the Oxygen Reduction Reaction through the Integration of O_2-Adsorbing Metal-Organic Frameworks on Nanocomposite Electrodes. *ACS Appl. Energy Mater.* **2018**, *1*, 5428−5436.
(19) Sang, X.; Zhang, J.; Peng, L.; Liu, C.; Ma, X.; Han, B.; Yang, G. Assembly of Mesoporous Metal-Organic Framework Templated by an Ionic Liquid/Ethylene Glycol Interface. *ChemPhysChem* **2015**, *16*, 2317−2321.
(20) Férey, G.; Serre, C.; Devic, T.; Maurin, G.; Jobic, H.; Llewellyn, P. L.; De Weireld, G.; Vimont, A.; Daturi, M.; Chang, J.-S. Why Hybrid Porous Solids Capture Greenhouse Gases? *Chem. Soc. Rev.* **2011**, *40*, 550−562.
(21) Sumida, K.; Rogow, D. L.; Mason, J. A.; McDonald, T. M.; Bloch, E. D.; Herm, Z. R.; Bae, T. H.; Long, J. R. Carbon Dioxide Capture in Metal-Organic Frameworks. *Chem. Rev.* **2012**, *112*, 724−781.
(22) Sumida, K.; Liang, K.; Reboul, J.; Ibarra, I. A.; Furukawa, S.; Falcaro, P. Sol-Gel Processing of Metal-Organic Frameworks. *Chem. Mater.* **2017**, *29*, 2626−2645.
(23) Sindoro, M.; Jee, A. Y.; Granick, S. Shape-Selected Colloidal MOF Crystals for Aqueous Use. *Chem. Commun.* **2013**, *49*, 9576−9578.
(24) Jeong, U.; Dogan, N. A.; Garai, M.; Nguyen, T.; Stoddart, J. F.; Yavuz, C. T. Inversion of Dispersion: Colloidal Stability of Calixarene Modified Metal-Organic Framework Nanoparticles in Non-Polar Media. *J. Am. Chem. Soc.* **2019**, *141*, 12182−12186.
(25) Tuninetti, J. S.; Rafti, M.; Azzaroni, O. Early Stages of ZIF-8 Film Growth: The Enhancement Effect of Primers Exposing Sulfonate Groups as Surface-Confined Nucleation Agents. *RSC Adv.* **2015**, *5*, 73958−73962.
(26) Rafti, M.; Allegretto, J. A.; Segovia, G. M.; Tuninetti, J. S.; Giussi, J. M.; Bindini, E.; Azzaroni, O. Metal−Organic Frameworks Meet Polymer Brushes: Enhanced Crystalline Film Growth Induced by Macromolecular Primers. *Mater. Chem. Front.* **2017**, *1*, 2256−2260.
(27) Allegretto, J. A.; Tuninetti, J. S.; Lorenzo, A.; Ceolín, M.; Azzaroni, O.; Rafti, M. Polyelectrolyte Capping As Straightforward Approach toward Manipulation of Diffusive Transport in MOF Films. *Langmuir* **2018**, *34*, 425−431.
(28) Allegretto, J. A.; Dostalek, J.; Rafti, M.; Menges, B.; Azzaroni, O.; Knoll, W. Shedding Light on the Dark Corners of Metal-Organic Framework Thin Films: Growth and Structural Stability of ZIF-8 Layers Probed by Optical Waveguide Spectroscopy. *J. Phys. Chem. A* **2019**, *123*, 1100−1109.
(29) Bétard, A.; Fischer, R. A. Metal-Organic Framework Thin Films: From Fundamentals to Applications. *Chem. Rev.* **2012**, *112*, 1055−1083.
(30) Shekhah, O.; Liu, J.; Fischer, R. A.; Wöll, C. MOF Thin Films: Existing and Future Applications. *Chem. Soc. Rev.* **2011**, *40*, 1081−1106.

(31) Huang, H.; Li, J. R.; Wang, K.; Han, T.; Tong, M.; Li, L.; Xie, Y.; Yang, Q.; Liu, D.; Zhong, C. An in Situ Self-Assembly Template Strategy for the Preparation of Hierarchical-Pore Metal-Organic Frameworks. *Nat. Commun.* **2015**, *6*, No. 8847.
(32) Shen, K.; Zhang, L.; Chen, X.; Liu, L.; Zhang, D.; Han, Y.; Chen, J.; Long, J.; Luque, R.; Li, Y.; Chen, B. Ordered Macro-Microporous Metal-Organic Framework Single Crystals. *Science* **2018**, *359*, 206−210.
(33) Peng, L.; Zhang, J.; Xue, Z.; Han, B.; Sang, X.; Liu, C.; Yang, G. Highly Mesoporous Metal-Organic Framework Assembled in a Switchable Solvent. *Nat. Commun.* **2014**, *5*, No. 4465.
(34) Avci, C.; Ariñez-Soriano, J.; Carné-Sánchez, A.; Guillerm, V.; Carbonell, C.; Imaz, I.; Maspoch, D. Post-Synthetic Anisotropic Wet-Chemical Etching of Colloidal Sodalite ZIF Crystals. *Angew. Chem., Int. Ed.* **2015**, *54*, 14417−14421.
(35) Koo, J.; Hwang, I. C.; Yu, X.; Saha, S.; Kim, Y.; Kim, K. Hollowing out MOFs: Hierarchical Micro- and Mesoporous MOFs with Tailorable Porosity via Selective Acid Etching. *Chem. Sci.* **2017**, *8*, 6799−6803.
(36) Kim, Y.; Yang, T.; Yun, G.; Ghasemian, M. B.; Koo, J.; Lee, E.; Cho, S. J.; Kim, K. Hydrolytic Transformation of Microporous Metal-Organic Frameworks to Hierarchical Micro- and Mesoporous MOFs. *Angew. Chem., Int. Ed.* **2015**, *54*, 13273−13278.
(37) DeCoste, J. B.; Rossin, J. A.; Peterson, G. W. Hierarchical Pore Development by Plasma Etching of Zr-Based Metal-Organic Frameworks. *Chem. - A Eur. J.* **2015**, *21*, 18029−18032.
(38) Ferguson, A.; Liu, L.; Tapperwijn, S. J.; Perl, D.; Coudert, F. X.; Van Cleuvenbergen, S.; Verbiest, T.; Van Der Veen, M. A.; Telfer, S. G. Controlled Partial Interpenetration in Metal-Organic Frameworks. *Nat. Chem.* **2016**, *8*, 250−257.
(39) Yang, J.; Zhang, Y. B.; Liu, Q.; Trickett, C. A.; Gutiérrez-Puebla, E.; Monge, M. A.; Cong, H.; Aldossary, A.; Deng, H.; Yaghi, O. M. Principles of Designing Extra-Large Pore Openings and Cages in Zeolitic Imidazolate Frameworks. *J. Am. Chem. Soc.* **2017**, *139*, 6448−6455.
(40) Shearer, G. C.; Chavan, S.; Bordiga, S.; Svelle, S.; Olsbye, U.; Lillerud, K. P. Defect Engineering: Tuning the Porosity and Composition of the Metal-Organic Framework UiO-66 via Modulated Synthesis. *Chem. Mater.* **2016**, *28*, 3749−3761.
(41) Cai, G.; Jiang, H. L. A Modulator-Induced Defect-Formation Strategy to Hierarchically Porous Metal−Organic Frameworks with High Stability. *Angew. Chem., Int. Ed.* **2017**, *56*, 563−567.
(42) Abdelhamid, H. N. Salts Induced Formation of Hierarchical Porous ZIF-8 and Their Applications for CO2 Sorption and Hydrogen Generation via $NaBH_4$ Hydrolysis. *Macromol. Chem. Phys.* **2020**, *221*, No. 2000031.
(43) Zacher, D.; Shekhah, O.; Wöll, C.; Fischer, R. A. Thin Films of Metal−Organic Frameworks. *Chem. Soc. Rev.* **2009**, *38*, No. 1418.
(44) Horcajada, P.; Serre, C.; Grosso, D.; Boissière, C.; Perruchas, S.; Sanchez, C.; Férey, G. Colloidal Route for Preparing Optical Thin Films of Nanoporous Metal-Organic Frameworks. *Adv. Mater.* **2009**, *21*, 1931−1935.
(45) Troyano, J.; Carné-Sánchez, A.; Avci, C.; Imaz, I.; Maspoch, D. Colloidal Metal-Organic Framework Particles: The Pioneering Case of ZIF-8. *Chem. Soc. Rev.* **2019**, *48*, 5534−5546.
(46) Armel, V.; Hannauer, J.; Jaouen, F. Effect of ZIF-8 Crystal Size on the O_2 Electro-Reduction Performance of Pyrolyzed Fe−N−C Catalysts. *Catalysts* **2015**, *5*, 1333−1351.
(47) Kumari, G.; Jayaramulu, K.; Maji, T. K.; Narayana, C. Temperature Induced Structural Transformations and Gas Adsorption in the Zeolitic Imidazolate Framework ZIF-8: A Raman Study. *J. Phys. Chem. A* **2013**, *117*, 11006−11012.
(48) Demessence, A.; Boissière, C.; Grosso, D.; Horcajada, P.; Serre, C.; Férey, G.; Soler-Illia, G. J. A. A.; Sanchez, C. Adsorption Properties in High Optical Quality NanoZIF-8 Thin Films with Tunable Thickness. *J. Mater. Chem.* **2010**, *20*, 7676.
(49) Tu, M.; Wannapaiboon, S.; Khaletskaya, K.; Fischer, Ra. Engineering Zeolitic-Imidazolate Framework (ZIF) Thin Film Devices for Selective Detection of Volatile Organic Compounds. *Adv. Funct. Mater.* **2015**, *25*, 4470−4479.
(50) Chu, Y.; Hou, J.; Boyer, C.; Richardson, J. J.; Liang, K.; Xu, J. Biomimetic Synthesis of Coordination Network Materials: Recent Advances in MOFs and MPNs. *Appl. Mater. Today* **2018**, *10*, 93−105.
(51) Kaur, H.; Mohanta, G. C.; Gupta, V.; Kukkar, D.; Tyagi, S. Synthesis and Characterization of ZIF-8 Nanoparticles for Controlled Release of 6-Mercaptopurine Drug. *J. Drug Deliv. Sci. Technol.* **2017**, *41*, 106−112.
(52) Park, K. S.; Ni, Z.; Cote, A. P.; Choi, J. Y.; Huang, R.; Uribe-Romo, F. J.; Chae, H. K.; O'Keeffe, M.; Yaghi, O. M. Exceptional Chemical and Thermal Stability of Zeolitic Imidazolate Frameworks. *Proc. Natl. Acad. Sci. U.S.A.* **2006**, *103*, 10186−10191.
(53) Huang, X. C.; Lin, Y. Y.; Zhang, J. P.; Chen, X. M. Ligand-Directed Strategy for Zeolite-Type Metal-Organic Frameworks: Zinc(II) Imidazolates with Unusual Zeolitic Topologies. *Angew. Chem., Int. Ed.* **2006**, *45*, 1557−1559.
(54) Xu, G.; Otsubo, K.; Yamada, T.; Sakaida, S.; Kitagawa, H. Superprotonic Conductivity in a Highly Oriented Crystalline Metal−Organic Framework Nanofilm. *J. Am. Chem. Soc.* **2013**, *135*, 7438−7441.
(55) Zhuang, J. L.; Terfort, A.; Wöll, C. Formation of Oriented and Patterned Films of Metal-Organic Frameworks by Liquid Phase Epitaxy: A Review. *Coord. Chem. Rev.* **2016**, *307*, 391−424.
(56) Avci, C.; Imaz, I.; Carné-Sánchez, A.; Pariente, J. A.; Tasios, N.; Pérez-Carvajal, J.; Alonso, M. I.; Blanco, A.; Dijkstra, M.; López, C.; Maspoch, D. Self-Assembly of Polyhedral Metal-Organic Framework Particles into Three-Dimensional Ordered Superstructures. *Nat. Chem.* **2018**, *10*, 78−84.
(57) Chocarro-Ruiz, B.; Pérez-Carvajal, J.; Avci, C.; Calvo-Lozano, O.; Alonso, M. I.; Maspoch, D.; Lechuga, L. M. A CO_2 Optical Sensor Based on Self-Assembled Metal-Organic Framework Nanoparticles. *J. Mater. Chem. A* **2018**, *6*, 13171−13177.
(58) Segovia, G. M.; Tuninetti, J. S.; Moya, S.; Picco, A. S.; Ceolín, M. R.; Azzaroni, O.; Rafti, M. Cysteamine-Modified ZIF-8 Colloidal Building Blocks: Direct Assembly of Nanoparticulate MOF Films on Gold Surfaces via Thiol Chemistry. *Mater. Today Chem.* **2018**, *8*, 29−35.
(59) Brunsen, A.; Calvo, A.; Williams, F. J.; Soler-Illia, G. J. A. A.; Azzaroni, O. Manipulation of Molecular Transport into Mesoporous Silica Thin Films by the Infiltration of Polyelectrolytes. *Langmuir* **2011**, *27*, 4328−4333.
(60) Tuninetti, J. S.; Rafti, M.; Andrieu-Brunsen, A.; Azzaroni, O. Molecular Transport Properties of ZIF-8 Thin Films in Aqueous Environments: The Critical Role of Intergrain Mesoporosity as Diffusional Pathway. *Microporous Mesoporous Mater.* **2016**, *220*, 253−257.
(61) Ariga, K.; Nishikawa, M.; Mori, T.; Takeya, J.; Shrestha, L. K.; Hill, J. P. Self-Assembly as a Key Player for Materials Nanoarchitectonics. *Sci. Technol. Adv. Mater.* **2019**, *20*, 51−95.
(62) Maji, S.; Shrestha, L. K.; Ariga, K. Nanoarchitectonics for Nanocarbon Assembly and Composite. *J. Inorg. Organomet. Polym. Mater.* **2020**, *30*, 42−55.
(63) Ariga, K. Nanoarchitectonics: Bottom-up Creation of Functional Materials and Systems. *Beilstein J. Nanotechnol.* **2020**, *11*, 450−452.
(64) Fonticelli, M. H.; Benítez, G.; Carro, P.; Azzaroni, O.; Salvarezza, R. C.; Gonzalez, S.; Torres, D.; Illas, F. Effect of Ag Adatoms on High-Coverage Alkanethiolate Adsorption on Au(111). *J. Phys. Chem. C* **2008**, *112*, 4557−4563.
(65) Azzaroni, O.; Schilardi, P. L.; Salvarezza, R. C. Templated Electrodeposition of Patterned Soft Magnetic Films. *Appl. Phys. Lett.* **2002**, *80*, 1061−1063.
(66) Azzaroni, O.; Fonticelli, M. H.; Benitez, G.; Schilardi, P. L.; Gago, R.; Caretti, I.; Vázquez, L.; Salvarezza, R. C. Direct Nanopatterning of Metal Surfaces Using Self-Assembled Molecular Films. *Adv. Mater.* **2004**, *16*, 405−409.

https://dx.doi.org/10.1021/acsanm.0c02376
ACS Appl. Nano Mater. XXXX, XXX, XXX−XXX

(67) Lowell, S.; Shields, J. E.; Thomas, M. A.; Thommes, M. Characterization of Porous Solids and Powders: Surface Area, Pore Size, and Density. In *Spr. Sci. & Bus. Med.*, 2004; Vol. *16*.
(68) Bard, A. J.; Stratmann, M.; Israel, R.; Masamichi, F.; Rusling, J. F. Encyclopedia of Electrochemistry. In *Modified Electrodes*, **2007**; Vol. *10*.
(69) Velasco, M. I.; Acosta, R. H.; Marmisollé, W. A.; Azzaroni, O.; Rafti, M. Modulation of Hydrophilic/Hydrophobic Character of Porous Environments in Metal−Organic Frameworks via Direct Polymer Capping Probed by NMR Diffusion Measurements. *J. Phys. Chem. C* **2019**, *123*, 21076−21082.
(70) Newton, M. R.; Morey, K. A.; Zhang, Y.; Snow, R. J.; Diwekar, M.; Shi, J.; White, H. S. Anisotropic Diffusion in Face-Centered Cubic Opals. *Nano Lett.* **2004**, *4*, 875−880.

https://dx.doi.org/10.1021/acsanm.0c02376
ACS Appl. Nano Mater. XXXX, XXX, XXX−XXX